Applications of RTM inverse scattering imaging conditions

N. D. Whitmore and Sean Crawley, PGS

Summary

Reverse time migration (RTM) is achieved by a forward and reverse time propagation of source and receiver wavefields respectively, followed by an imaging condition. The quality of the image from any RTM implementation depends directly on the method's ability to separate the true reflection data from the backscattered correlation noise between the source and receiver wavefields. In this paper we demonstrate the application of an inverse scattering imaging condition that significantly reduces this backscattered correlation noise and results in a much higher quality subsurface image than is achieved by typical RTM imaging conditions.

Introduction

Reverse time imaging (RTM) constructs the image from numerically synthesized subsurface incident and reflected wavefields. A representation of the seismic source and the reversed time reflection seismogram are used as boundary conditions in a seismic modeling framework to simulate the time history of these data in the subsurface. An approximation of the reflectivity of the earth is then generated by appropriately combining these images at locations where these two wavefields are in phase at the time of reflection in the subsurface. There are a variety of methods for computing the image, but often the method of choice is based on a cross-correlation between the source and receiver wavefields (Claerbout, 1971), which is the time integration of the forward and reverse time wavefields, potentially scaled by a normalization factor which corrects for source power, transmission, illumination and acquisition effects.

Unfortunately, RTM correlation methods can be negatively affected by backscattered and turning waves in the modeling process, which causes the incident and reflected wavefields to be in phase at locations that are not the reflection points (see Figure 1). This results in strong correlation noise in the seismic image. We demonstrate this using a synthetic model. Figure 2 shows the velocity model and the complex ray paths and wavefronts that are associated with this correlation noise (model courtesy BP, Billette, F., and S. Brandsberg-Dahl, 2005). The source and receiver wavefields are in phase everywhere along these ray paths. The corresponding RTM correlation image is shown in Figure 3, where we see that the low wavenumber correlation artifacts occur where there are complex scattered and turning wave raypaths.

Typical means of addressing this correlation noise is to reduce these artifacts by conditioning the modeling process (e.g. smoothing, impedance matching, damping). However, conditioning the model can introduce propagation errors, and thus there is a tradeoff between artifact reduction and imaging accuracy. Also, model conditioning typically does not address turning waves or high angle reflections. Post processing of the RTM image with spatial reject filters is often used to attenuate the low wavenumber noise and can reduce the near dc component of the noise. (e.g. Guitton,et al., 2006). However, these methods need to be used with care and must properly treat the velocity dependent wavenumber variations in the depth image.

In the last few years, more attention has been placed on using improved imaging conditions designed to reduce the imaging noise by using directional information computed directly from the data - for example by using multi-dimensional transforms, time and spatial lags or direction vectors from differential operators applied to the wavefield (e.g. Yoon and Marfurt, 2006). In this paper, we present a an imaging process based on a generalized inverse scattering imaging condition (Stolk, DeHoop, and Opt'Root, 2009). This method is based on an elegant inverse scattering theory, in which the backscattered waves are attenuated by using the combination of two separate images: one based on the product of the time derivatives of the incident and reflected wavefields and the other based on the product of the spatial gradients of the incident and reflected wavefields. These images are then combined to produce the final inverse scattering image.

In this paper we discuss our implementation of these concepts and demonstrate their effectiveness on both synthetic and field data.

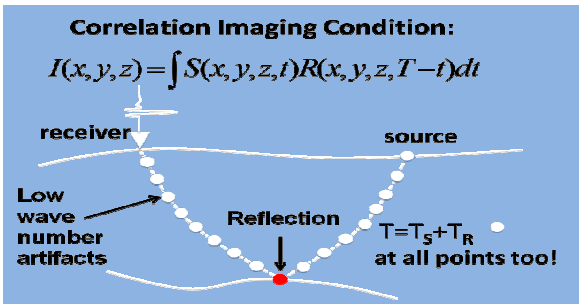

Figure 1. RTM correlation can map data at all scattering points along the source-receiver ray paths, not just at the reflector.

DOI http://dx.doi.org/10.1190/segam2012-0779.1

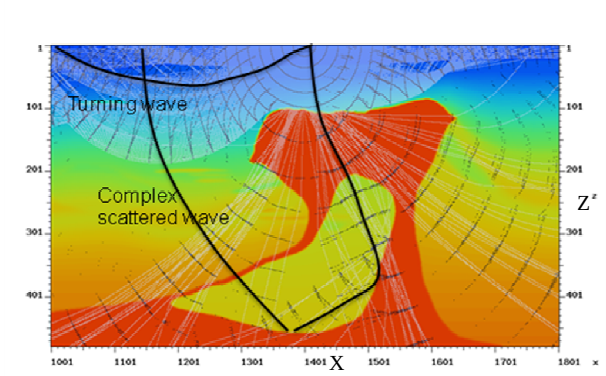

Figure 2. Velocity model with raypaths and wave fronts, with a turning ray and complex scattered wave highlighted (model, courtesy BP)

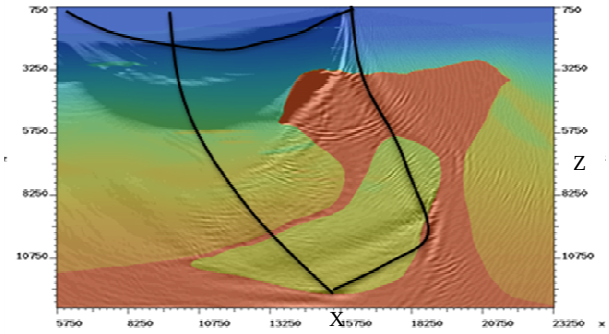

Figure 3. RTM Correlation Image. Note the low frequency artifacts come both from backscattering from the salt and turning waves. (Dark lines indicate selected ray paths)

Theory

As we see from the previous section, much of the contamination of the RTM image is caused by the spatial correlation of the backscattered noise of the source and receiver wave-fields. We want to design imaging conditions that penalize this noise, and at the same time preserve the desired reflectivity image. In order to achieve this, we note that we can approximate the ray parameter of a wavefield from the following differential operator:

$$\mathbf{p} = \frac{\nabla U(\mathbf{x},t)}{\left[\frac{\partial U(\mathbf{x},t)}{\partial t}\right]} \qquad \mathbf{x} = (x, y, z) \tag{1}$$

In principal, this approximation can be applied to either source or receiver wavefields, provided that the wavefield events are single valued. In the case of multi-valued wavefields, some form of separation may be required to compute a direction vector of a wavefield, which for example, can be achieved through a local space-time operator. We do not require this in the actual inverse scattering condition – we simply note that directional information is contained in the combination of the time derivative and gradient of a wavefield. If we define the source and receiver wavefields as *S(x,t)* and *R(x,t)* respectively, the we can represent the respective source and receiver ray parameters:

$$\mathbf{p}_S(\mathbf{x},t) \approx \frac{\nabla S(\mathbf{x},t)}{\left[\frac{\partial S(\mathbf{x},t)}{\partial t}\right]} \tag{2}$$

$$\mathbf{p}_R(\mathbf{x},t) \approx \frac{\nabla R(\mathbf{x},t)}{\left[\frac{\partial R(\mathbf{x},t)}{\partial t}\right]} \tag{3}$$

We note that this is only a far field plane wave approximation, but it helps to give insight into the inverse scattering imaging condition. Note that if we multiply the time derivative terms by their respective ray parameters, and form a dot product we get the following equation.

$$[\mathbf{p}_S(\mathbf{x},t)\frac{\partial S(\mathbf{x},t)}{\partial t}] \bullet [\mathbf{p}_R(\mathbf{x},t)\frac{\partial R(\mathbf{x},t)}{\partial t}] \tag{4}$$
$$\approx \nabla S(\mathbf{x},t) \bullet \nabla R(\mathbf{x},t)$$

Using the following ray parameter relations

$$|\mathbf{p}_S| = |\mathbf{p}_R| = \frac{1}{V(\mathbf{x})} \;;\; \cos(\mathbf{p}_S, \mathbf{p}_r) = \frac{\mathbf{p}_S \bullet \mathbf{p}_R}{|\mathbf{p}_S||\mathbf{p}_R|} \tag{5}$$

we obtain the following equation:

$$\frac{\partial S(\mathbf{x},t)}{\partial t}\frac{\partial R(\mathbf{x},t)}{\partial t}\cos(\mathbf{p}_S,\mathbf{p}_R)\,A(\mathbf{x}) / V^2(\mathbf{x}) \tag{6}$$
$$= \nabla S(\mathbf{x},t) \bullet \nabla R(\mathbf{x},t)$$

where the ***A(x)*** is a positive function that is introduced to account for the far field approximations, which could also depend on ray parameters, anisotropy, transmission effects, spreading, acquisition, etc.

Note $B \equiv \cos(\mathbf{p}_S,\mathbf{p}_R)A(\mathbf{x})/V^2(\mathbf{x})$ can be considered as an angle dependent scaling function used to relate the time derivative wavefield product to the product of the spatial gradients. Perhaps the most important aspect of this is that this combined weighting function is either positive or negative, depending on the ray parameter directions.

DOI http://dx.doi.org/10.1190/segam2012-0779.1

This gives rise to the following important fact:

When $\cos(\mathbf{p}_S, \mathbf{p}_R) > 0$ the data is backscattered or turning wave energy; this is because the source and receiver wavefields are traveling in the same direction.

While this is only an approximation, it gives motivation for creating two separate imaging conditions and then combining the results in a way to attenuate the "in phase" components of the image, which are the cause of the correlation noise. These imaging conditions are

$$I_{\nabla}(\mathbf{x}) = \int [\nabla \psi_s(\mathbf{x},t) \bullet \nabla \psi_r(\mathbf{x}, T-t)] dt \quad (7)$$

$$I_{dt}(\mathbf{x}) = \int \frac{1}{V^2(x)} \left[\frac{\partial}{\partial t} \psi_s(\mathbf{x},t) \frac{\partial}{\partial t} \psi_r(\mathbf{x}, T-t) \right] dt \quad (8)$$

where ψ_S and ψ_R are the source and receiver wavefields scaled by the $(1/\omega)^{\alpha}$ in the frequency domain and where α is chosen to frequency scale the time derivatives of the wavefields and apply the appropriate frequency weighting for the 2D or 3D dimensionality of the data. The final inverse scattering image is computed as the normalized sum of these two images:

$$I(\mathbf{x}) = \frac{1}{W(\mathbf{x})} [I_{\nabla}(\mathbf{x}) + B(\mathbf{x}) I_{dt}(\mathbf{x})] \quad (9)$$

$W(\mathbf{x})$ is an approximate amplitude correction, which could include source power, transmission effects, etc. $B(\mathbf{x})$ serves the role of the required amplitude weighting to attenuate the backscattered energy. For scaling after forming the stack of all images, $B(\mathbf{x})$ is a scalar function, whereas in the prestack domain (on individual shot migrations or angle gathers), $B(\mathbf{x})$ is typically angle dependent (related to the weighed scaling by $\cos(\mathbf{p},\mathbf{q})$ in equation 6).

Example 1. Synthetic BP Model:

The inverse scattering imaging was applied to the data from the BP model discussed in Figures 2 and 3. Two independent images were created from a single synthetic shot, the first was computed using equation (7) and the second was computed from equation (8). The subsequent images were weighted and stacked via the computations described in equation (8). The normalization field $B(\mathbf{x})$ was computed from the low wavenumber components of the respective "dt" and "grad" images and is not constant.

The images from the shot are shown in Figure 4. The inverse scattering imaging condition, $I(\mathbf{x})$, has significantly reduced the backscattered noise - demonstrating the effectiveness of this method in reducing RTM imaging artifacts in the migration of a single shot.

(4a) Image from gradients

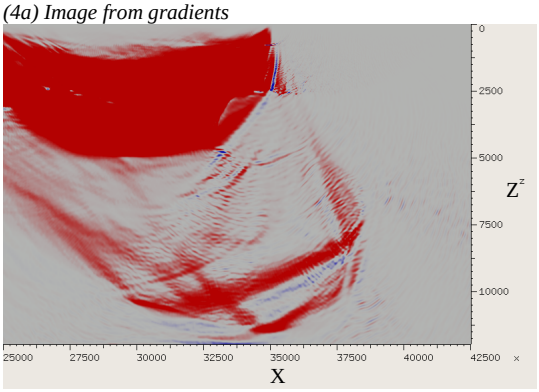

(4b) Image from time derivatives

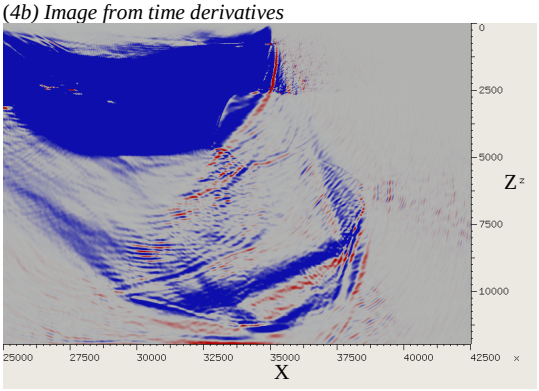

(4c) Inverse scattering image from the weighted sum

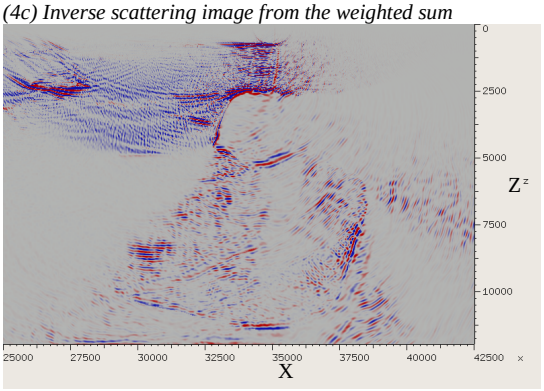

Figure 4. Images of a single shot migration (a) is from the product of the gradient terms as described by equation (7), (b) is from the product of time derivatives described by equation (8) and (c) is the weighted sum described by equation (9).

While only the image from a single shot is shown here, this imaging condition can be applied shot by shot and the final image constructed by summation over shots, which then produces the final summed image. However, an alternative is to construct summed images by applying the imaging conditions (7) and (8) for each shot, accumulating separate stacks for each imaging condition and then the results can

DOI http://dx.doi.org/10.1190/segam2012-0779.1

be subsequently summed to produce a final stacked inverse scattering image, This is demonstrated in Figure 5, where the low wavenmber backscattered artifacts have been significantly reduced in the inverse scattering image.

(5a) Sum of the gradient shot images

(5b) Sum of the time derivative images

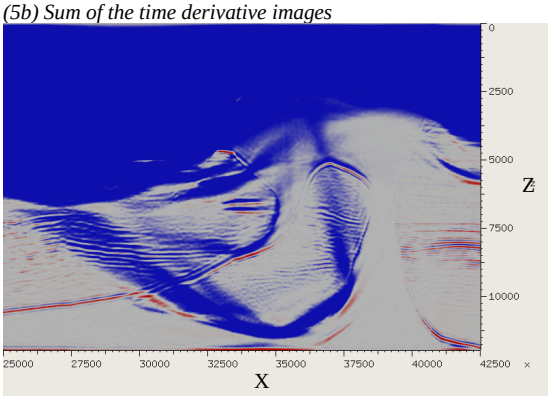

(5c) Inverse scattering image -weighted sum of (5a) and (5b)

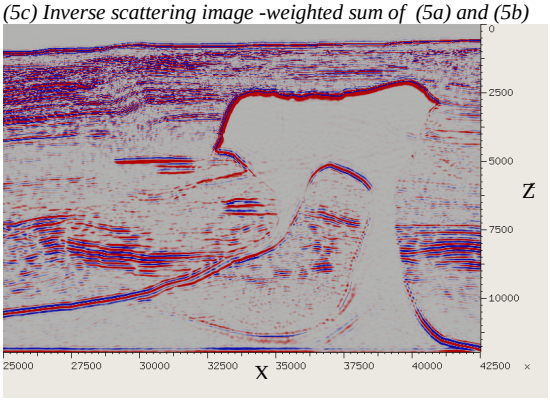

Figure 5. Images for the BP synthetic constructed first by computing the gradient images and time images for each shot and summing (5a), then computing time derivative images for each shot and summing (5b) and computing a weighted stack of these (5c) to produce the final image.

Example 2. RTM of dual-sensor data

We applied the same process to dual-sensor shot records from offshore Africa. $I_{\Delta}(\mathbf{x}), I_{dt}(\mathbf{x})$ and the inverse scattering image, $I(\mathbf{x})$, are shown in Figure 6 below.

(6a) Sum of the gradient shot images

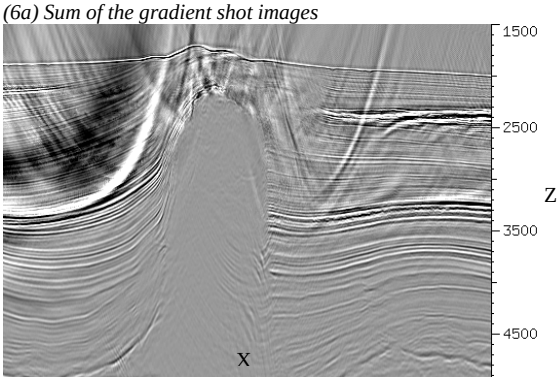

(6b) Sum of the time derivative images

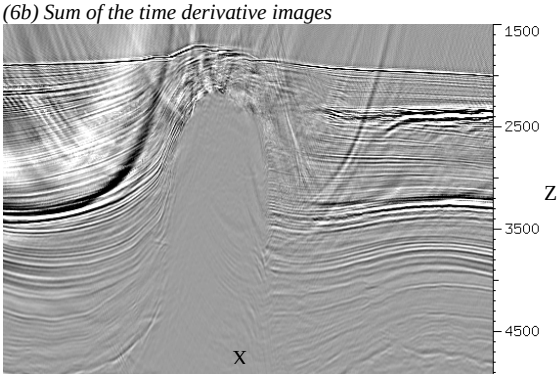

(6c) Inverse scattering image - weighted sum of (6a) and (6b)

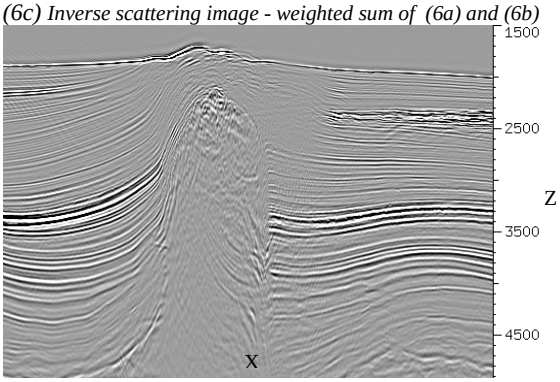

Figure 6 Deep water images (offshore Africa) constructed by computing the gradient for each shot and summing (6a), then computing time derivative for each shot and summing (6b) and computing a weighted stack of these, which is the inverse scattering image (6c).

DOI http://dx.doi.org/10.1190/segam2012-0779.1

RTM angle gathers (Example 2 continued)

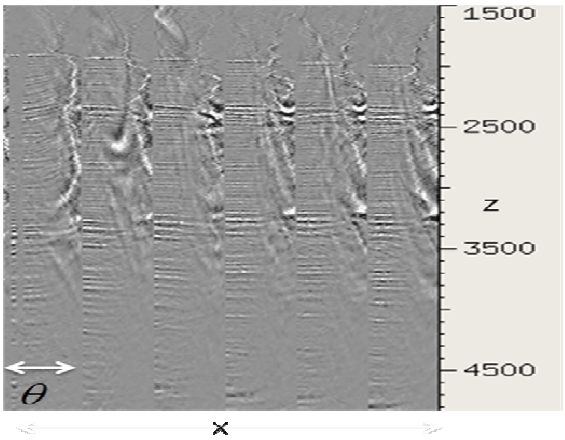

Figure 7 Angle gathers from gradient image

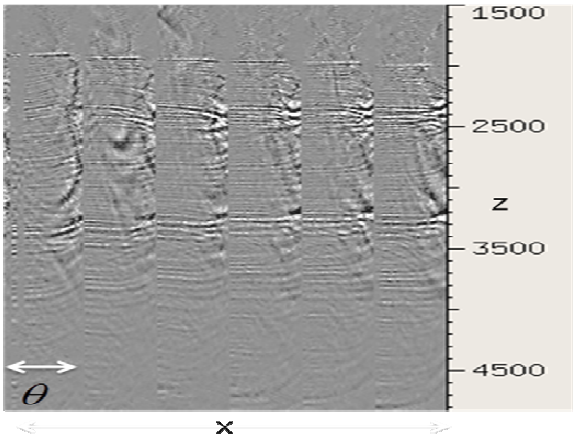

Figure 8 Angle gathers from time derivative image

While beyond the scope of this paper, we note that RTM angle gathers can also be created using the computed direction vectors and possibly structural dip (e.g. Yoon, et al., 2011). The inverse scattering imaging conditions can be applied to each angle independently. Figures 7, 8 and 9 show an example of selected angle gathers from the offshore Africa data, using the $I_{\Delta}(\mathbf{x}), I_{dt}(\mathbf{x})$ and then inverse scattering equation (9) is applied to each angle. Computing the imaged $I(\mathbf{x})$ angle gathers require the weighting function $B(x)=B(x,\theta)$ to depend on both x and angle.θ The final angle gathers are shown in Figure 9.

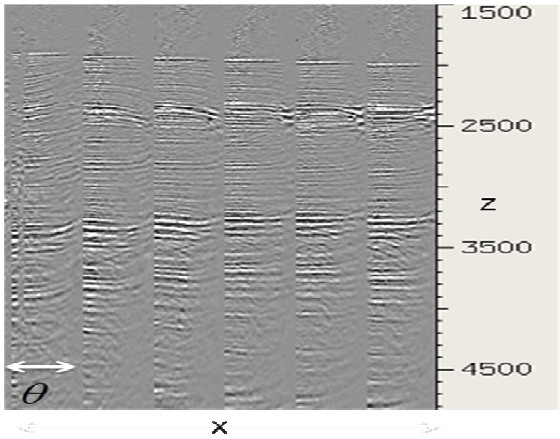

Figure 9. Angle gathers from the inverse scattering condition, which is the weighted sum of the gathers shown in Figures 7 and 8.

In summary, we observe that the inverse scattering imaging condition can be applied in all of the cases discussed above (individual shots, stacked images and angle gathers). Furthermore, the inverse scattering type imaging conditions produce much higher quality images than do standard correlation methods.

Conclusions

Reverse time migration is a powerful imaging tool, but can be plagued with strong backscattered artifacts that must be removed from the data to produce an optimal subsurface image. We demonstrate an inverse scattering imaging condition that is a weighted sum of: (1) the dot products of the gradients of the incident and scattered fields and (2) the product of the time derivatives of the incident and reflected fields. This method significantly reduces the artifacts in the imaged data in both the synthetic and field data. This imaging condition preserves true reflection data while at the same time tends to annihilate the backscattered noise.

This method can be implemented in the shot domain, the RTM angle domain or after first separately accumulating the component gradient and time derivative images and then applying the inverse scattering imaging condition to these stacked volumes.

Acknowledgments

We thank PGS for permission to publish this paper and the use of the dual-sensor data from offshore Africa and the assistance of the PGS processing group in the UK. We also thank Maarten de Hoop for suggesting this type of approach for imaging conditions.

DOI http://dx.doi.org/10.1190/segam2012-0779.1

http://dx.doi.org/10.1190/segam2012-0779.1

EDITED REFERENCES

Note: This reference list is a copy-edited version of the reference list submitted by the author. Reference lists for the 2012 SEG Technical Program Expanded Abstracts have been copy edited so that references provided with the online metadata for each paper will achieve a high degree of linking to cited sources that appear on the Web.

REFERENCES

Billette, F., and S. Brandsberg-Dahl, 2005, The 2004 BP velocity benchmark: 67th Conference and Exhibition, EAGE, Extended Abstracts, B035.

Biondi, B., and G. Shan, 2002, Prestack imaging of overturned reflections by reverse-time migration: 72nd Annual International Meeting, SEG, Expanded Abstracts, 1284–1287.

Claerbout, J. F., 1971, Toward a unified theory of reflector mapping: Geophysics, **36**, 467–481.

Guitton, A., B. Kaelin, and B. Biondi, 2007, Least-squares attenuation of reverse-time-migration artifacts: Geophysics, **72**, no. 1, S19–S23.

Stolk, C. C., M. V. de Hoop, and T. Op't Root, 2009, Linearized inverse scattering based on seismic reverse-time migration: Proceedings of the Project Review, Geo-Mathematical Imaging Group (Purdue University, West Lafayette IN), 91–108.

Yoon, K., M. Guo, J. Cai, and B. Wang, 2011, 3D RTM angle gathers from source wave propagation direction and dip of reflector: 81st Annual International Meeting, SEG, Expanded Abstracts, 3136–3140.

Yoon, K., and K. J. Marfurt, 2006, Reverse-time migration using the Poynting vector: Exploration Geophysics, **37**, 102–107.